Effect of deuterium irradiation on ATJ graphite boronized in NSTX-U

F. Bedoya[1*], J.P. Allain[2], F.J. Dominguez[3] and P. Krstic[4]

[1]*Plasma Science and Fusion Center, Massachusetts Institute of Technology, Cambridge, MA 02139 USA*
[2]*Department of Nuclear, Plasma, and Radiological Engineering, University of Illinois, Urbana, IL 61801*
[3]*Max-Planck-Institute for Plasma Physics, Boltzmannstrasse 2, 85748 Garching, Germany*
[4]*Institute for Advanced Computational Science, Stony Brook University, Stony Brook, NY 11749*

Abstract

Boronization has been recently used in the National Spherical Torus-Upgrade (NSTX-U) as main first wall conditioning technique. The technique decreased the oxygen impurity content in the plasma as well as the O concentration on the Plasma Facing Components (PFC) as measured with an *in-vacuo* probe. Core samples were manufactured from tiles extracted from the tokamak for *post-mortem* and controlled studies in the laboratory at the end of the experimental campaign. Low fluence ($3.0x10^{16}$ cm^{-2}) D_2^+ and ($3.5x10^{17}$ cm^{-2}) Ar^+ irradiations were performed on the samples using different fluence steps and the surface chemistry was investigated with X-ray Photoelectron Spectroscopy (XPS) in between irradiations. Classical Molecular Dynamics (CMD) simulations with reactive force field (REAXFF) were used to investigate the chemistry of the B-C-O-D system. The results suggest that boron coatings retain oxygen by forming oxidized boron states only in the presence of deuterium plasmas. In contrast, argon irradiations removed such oxides. Additionally, measurements of the residual gases in the chamber, performed during the irradiations, indicates potential retention of D by the B coatings as predicted by the CMD

results. A good degree of qualitative agreement was observed between the experimental and computational data. This set of results provides further details to understand the how boron coatings help to improve plasma performance in tokamaks with graphite PFC, which can later lead to optimization and enhancement of this type of conditioning.

1. Introduction

Tokamak devices remain one of the most promising configurations to reliably harvest energy from fusion reactions through magnetic confinement of plasmas[1]. The density, temperature and energy confined dictate the plasma performance and greatly affect the overall performance of the machine[2]. Multiple studies have shown the strong effect that the Plasma Facing Components (PFC) and their chemical state have on plasma performance[3–6]. As a consequence, several methods of PFC conditioning have been developed and optimized to improve this performance [3,7,8]. The plasma assisted deposition of thin films of C, Si, Ti or B on PFC has been extensively used in different machines to improve the plasma behavior and protect the PFC [9]. In general, these coatings reduce physical and chemical sputtering and the amount of plasma impurities due to high sticking coefficients to the surface and oxide formation and adhesion [9–11] .

The National Spherical Torus Experiment Upgrade (NSTX-U) is a spherical tokamak with carbon-based PFC [12–14]. During the FY2016 experimental campaign, boronization was used as the main PFC conditioning technique in NSTX-U [13,15]. Boron was deposited using a DC glow of He and deuterated Trimethyl boron (d-TMB)[15]. This conditioning yielded boron rich

coatings several fractions of nanometers thin that enabled plasma performance improvements shortly after their application[6,12] with the intention to reduce the overall oxygen impurity content by water and oxygen reduction at the boronized graphitic surface. However, the performance worsen with increasing plasma exposures requiring frequent subsequent boronizations. To understand the dynamic interactions of impurity fluxes to the boronized graphitic surfaces and their evolution under D plasma irradiation, *in-situ* characterization was conducted with the Materials Analysis Probe (MAPP) PMI diagnostic and computational simulations of the B-C-O-D system dynamics and chemistry were carried out using Classical Molecular Dynamics (CMD) with reactive force field potentials (ReaxFF) [6,16,17]. This work complements these studies by examining NSTX-U tiles *post-mortem* and conducting controlled *in-situ ex-vessel* surface characterization studies in close comparison with computed results (including oxygen and deuterium accumulation in the samples) to expand on MAPP results and provide a deeper fundamental understanding of D and impurity retention, surface chemistry and physics of boron-conditioned graphite.

Post-mortem analysis to investigate the accumulated effects of B conditioning and D plasma exposures during the campaign, and as part of the broader PFC investigation effort of the NSTX-U team, consisted of removing several tiles from NSTX-U and cored samples extracted from the these. This work reports the experiments performed under *ex-vessel* controlled laboratory conditions in the IGNIS facility at University of Illinois, including low fluence deuterium and argon irradiation in combination with X ray photoelectron and gas spectroscopy analysis on one

of the boronized graphite cored samples. Details on the experimental settings and measurements are provided in section 2.1 and 2.2.The CMD calculation uses the Reactive Force Field (ReaxFF) bond order potential adapted to the B-C-O-D system, Details of the calculations are depicted in section 2.3.

In the same way, Section 3 is dedicated to the discussion of the experimental and theoretical data. Sections 3.1 and 3.3 present our analysis of the results obtained in the laboratory using XPS and gas analysis respectively, whereas section 3.2 presents the results obtained with the CMD simulations.

2. Experimental Methods

2.1 Post-mortem analysis of NSTX-U tile surfaces

A *post-mortem* methodology was earlier designed by Taylor and Allain with NSTX staff for graphite-based reactive interfaces to provide surface characterization of the "realistic" material containing the overall plasma exposure history after thousands of shots in NSTX-U [18,19]. The methodology consists of coring samples from tiles extracted from the NSTX device at various locations known to have different PMI conditions (e.g. far scrape-off-layer, private flux region, etc…) transferred to high-resolution multi-analysis surface characterization tools. Although samples are exposed to atmosphere, Allain et al. demonstrated that a passivated layer effectively protects the *plasma-induced surface chemistry* below and can be excavated with energetic Ar^+ ions carefully sequenced between surface composition measurements *in-situ.* Therefore, one can

distinguish with high reliability the passivated surface region compared to the active region of interest in the relevant core-level XPS spectra. Here we define "*in-situ"* in terms of characterization of the sample surface *in place* of surface irradiations.

Three tiles were removed from different locations of NSTX-U (Inner Lower Divertor (ILD), Outer Lower Divertor (OLD) and Center Stack Shoulder (CSS)) at the end of the experimental campaign. PFC in NSTX-U are manufactured with ATJ (lower divertor tiles) and POCO (center stack shoulder) graphite. These locations were intentionally selected to investigate PFC at locations subjected to different plasma conditions during the experimental campaign. In this case, the OLD is the common location of the Outer Striking Point (OSP), and is, in general, considered as the main source of impurities in diverted tokamaks. In the same way, the CCS location is the place where the Inner Striking point ISP is usually placed, and, according to multiple studies in material migration, is the destination of most of the eroded particles. Lastly, the ILD usually exhibits a high concentration of gas neutrals and low ion fluxes [20,21].

In the development of the campaign the tiles were exposed to multiple boronizations under different configurations (gas injectors and electrodes as shown in Ref [15]) and conditions, in addition to thousands of deuterium plasma shots, Helium Glow Discharge Cleaning (HeGDC) procedures and additional plasma glows with Ne. Details on *in-situ* chemical analysis of samples exposed to boronizations in NSTX-U and on the procedure itself can be found in Ref [6,15].

Cores with 1 cm in diameter were extracted from each tile for different characterizations e.g. SIMS, XPS, RBS. *Post-mortem* characterization of one core from each tile revealed a lower

concentration of oxides in the CSS sample than those from the OLD or ILD after cleaning with Ar^+ ions. As a consequence, this sample was also used for further D_2^+ irradiations and the measurements presented in this work were obtained with one of the CSS cores.

2.2 In-situ surface chemistry characterization

The Ion-Gas and Neutrals Interactions with Surfaces (IGNIS) facility is an *in-situ, in-operando* surface modification and characterization facility at University of Illinois. The system exposes samples between low and moderate levels of hydrogen isotope and helium fluences and includes several surface characterization techniques including: X-ray Photoelectron Spectroscopy, Ion Scattering Spectroscopy and Thermal Desorption Spectroscopy.

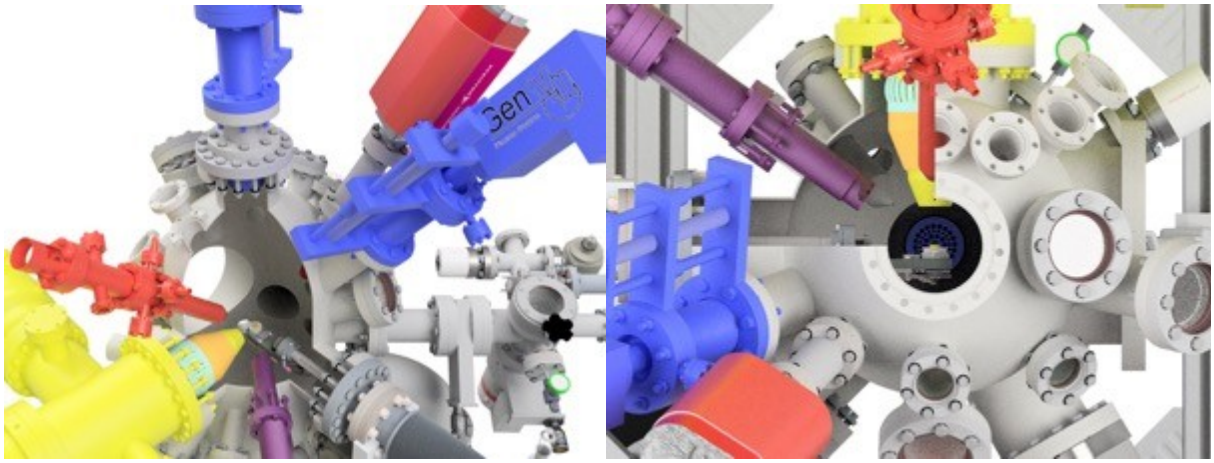

(a) **(b)**

Figure 1. Renders of the IGNIS facility at the University of Illinois, (a) shows the sample in the irradiation position, the blue elements are Tectra sources, the red elements are low flux ion guns for ion based diagnostics, (b) shows the sample in the XPS analysis position, here the yellow element is the energy analyzer while the XRS is shown in purple.

One unique advantage of IGNIS, compared with similar facilities is the possibility to characterize the chemistry of a surface during irradiation under harsh environmental conditions of

temperature (e.g. 77K-1000K), energetic particle bombardment (10-1000 eV) and high pressure (due to an additional background gas or to a high working pressure to the presence of gas neutrals) close to 5 mTorr, mimicking plasma-material interaction in fusion devices. This is possible thanks to an advanced differentially pumped hemispherical analyzer (modified SPECS 150 NAP). The design of the analyzer includes two differential pumping stages, each one with a 600 L/sec turbo-molecular pump. These stages are separated by a set of mechanical diaphragms that isolate the analysis chamber from the section of the analyzer that contains the Micro Channel Plate detector.

This configuration can lead to pressure differences close to four orders of magnitude between the analysis and the MCP chambers. Additionally, the analyzer has an ultimate energy resolution of 2.5 meV [22]. To perform high-pressure XPS, IGNIS consists of a water-cooled dual anode SPECS XR-50 high-pressure X-Ray Source (XRS), similarly to the analyzer, differentially pumped to perform at pressures as high as 5 mTorr. To meet high-pressure requirements in the XRS the volume that contains the thoriated W filaments is isolated from the IGNIS analysis chamber [22]. For the irradiations included in this work, we used a Tectra Gen II plasma source. This is a microwave source capable of operating with noble and reactive gases [23]. Ion fluxes close around 10^{14} $cm^{-2}s^{-1}$ with Ar^{+} and 10^{13} $cm^{-2}s^{-1}$ for D_2^{+}. The vacuum quality and the presence of residual gas impurities are monitored in IGNIS with a high-pressure Residual Gas Analyzer

(RGA) (Inficon Transpector® XPR3). This device can operate at pressures as high as 5 mTorr and record the m/q signals from 2 to 100 amu with a resolution of 1 amu [24].

The sample was loaded in a custom designed holder and pumped down to 10^{-7} Torr for its insertion into the analysis chamber. The IGNIS analysis chamber usually has a base pressure of 10^{-8} Torr with a partial pressure of water close to 10^{-11} Torr. Initial XPS baseline spectra were then collected, this group of data includes a survey scan and three region scans (B1s, C1s and O1s). Following the first characterization several irradiations were performed with the Tectra source using 1 keV Ar^+. The first irradiations totaled $3.5x10^{17}$ ions.cm^{-2} fluence and were done in incremental steps, starting from $1.0x10^{15}$ ions.cm^{-2} and with a final value after the last irradiation of $1.0x10^{17}$ ions.cm^{-2}. Additional XPS data groups were collected in between irradiations including the same regions mentioned above. Following the Ar^+ treatment three D_2^+ irradiations of $2.0x10^{16}$ ions.cm^{-2} (250 eV/amu) were performed on the sample. As before, XPS data were collected at the end of each irradiation. Finally, the sample was exposed to two more Ar^+ irradiations of $1.0x10^{17}$ ions.cm^{-2} fluence each, XPS data was again measured following each exposure. A quadrupole mass spectrometer (QMS) was used during all the irradiations to collect data that would reveal possible emission of species from the sample when exposed to Ar^+ or D_2^+. The QMS was set to follow amongst others D_2, H_2O, O, O_2 and D_2O (4, 18, 16, 32 and 20 amu). Unfortunately, masses 3 and 19 amu (HD and HDO) were not recorded during the experiment, thus making it challenging to quantify the total desorbed D (emission through these two channels usually amounts to over 50% of the total absorbed D in ATJ graphite [25]). To evaluate the

dependence of each one of the m/q values on the ion flux, the current induced by the ion beam was measured with a pico-amp meter connected in series to the samples manipulator. Each partial pressure in time could be then compared with the same variation of the ion flux. The experimental procedure is shown schematically in figure 2.

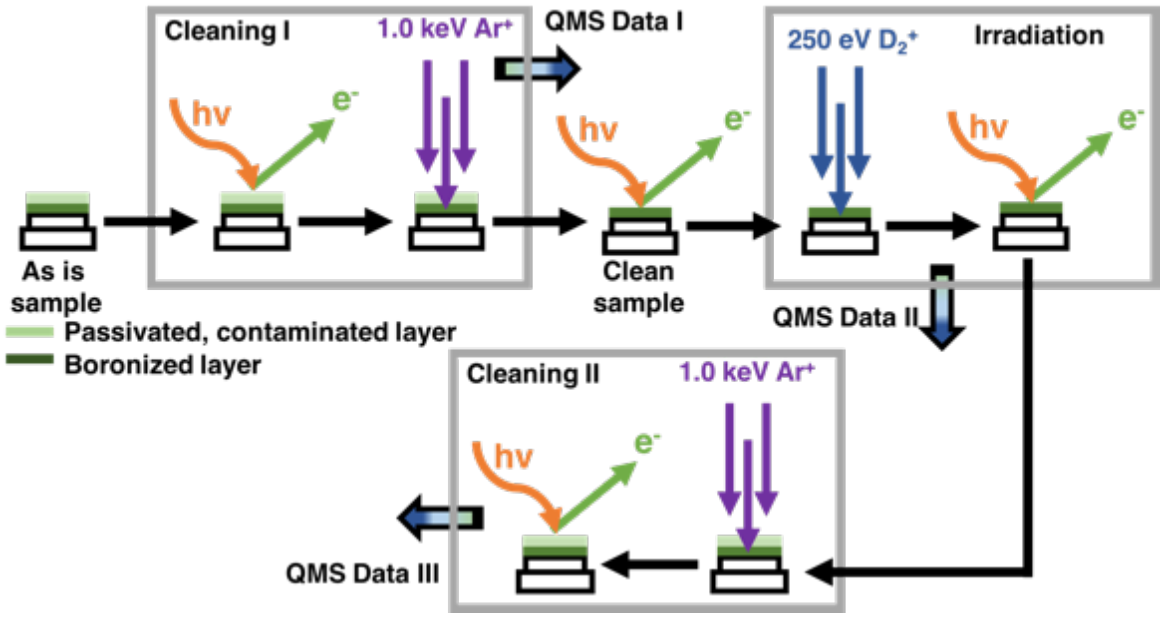

Figure 2. Schematic representation of the experimental procedure. XPS and QMS data was acquired during the different stages i.e. two Ar^+ cleaning and one D_2^+ irradiation steps.

2.3 Computational methods

Our atomistic simulations are based on Classical Molecular Dynamics, with use of the Reactive Force Field (ReaxFF) Bond Order potential [26,27] adapted to B-C-O-D mixture of materials and implemented in the Large Scale Atomic/Molecular Massively Parallel Simulator (LAMMPS) [28]. The ReaxFF method applies the Electronegative Equalization Method (EEM)[29,30] at each time step. This is particularly important in the presence of mutually polarizable materials

such as boron, and oxygen. We verified [10,11,17,31] the CMD calculations by Quantum-Classical Molecular Dynamics (QCMD), using approximate Self Consistent Charge Tight Binding Density Functional Theory (SCC-DFTB) [32] to compute electronic motions in the adiabatic limit of nuclear motion. The procedure for formation, annealing and optimization of the computational cell is explained in detail in Ref [10,11,31].

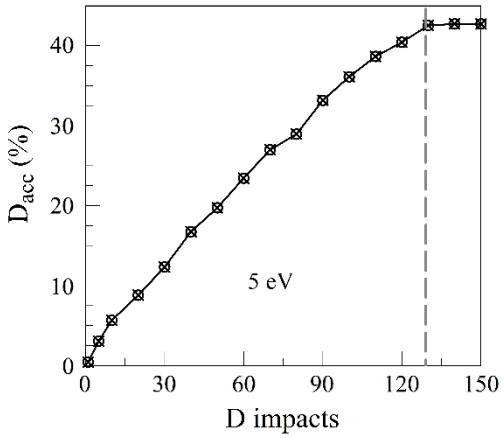

Figure 3. Percentage of implanted D as function of number of D impacts needed to prepare the BCO:D surface at 5 eV. The saturation of D is reached at 43% of D.

We use a computational cell of about 400 atoms for various amorphous mixtures of B, C, and O. Boronized and oxidized systems are created by random substitution of carbon atoms to the desired atomic concentrations, estimated by the experiment to be atomic composition of (20, 40, 40) % for B, C, O respectively. The mixtures are then annealed and finally thermalized to 300 K and energy optimized with periodic boundary conditions in the x-y directions, following the procedure of Krstic *et al[31,33]*.

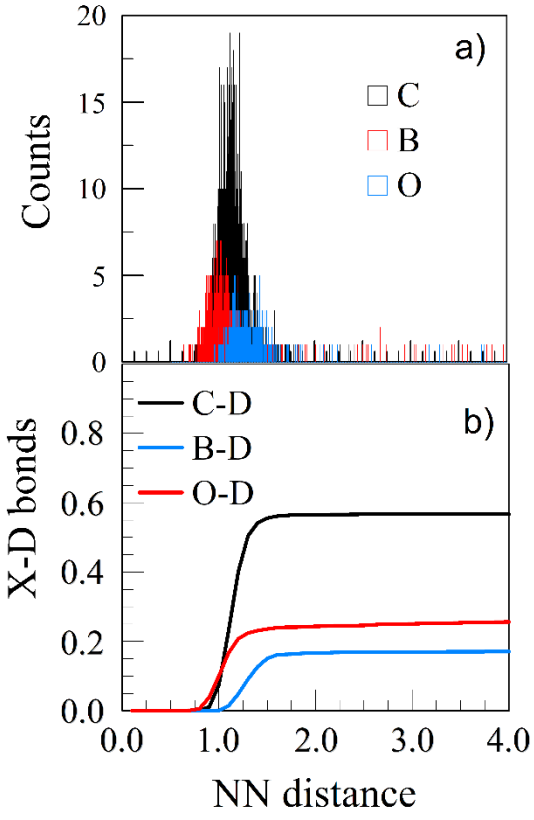

Figure 4. a) Histogram and b) cumulative distribution of the X-D (X=B,C,O) NN distances of the pristine BCO surface replicas bombarded over 3000 times with 5 eV D. Cumulative distribution functions show the percentages of X-D bonds, 57 % of C-D, 26 % of O-D, and 17 % of B-D.

This procedure allows the formation of complexes with the chemical properties studied in this paper. Additional reformation of the chemical complexes evolves upon bombardment with D atoms, as explained below. To take into account typical experimental conditions of the accumulated deuterium, the B-C-O cells of total of 400 atoms were prepared by cumulative bombardment with 5 eV D atoms, reaching various atomic concentrations of D. The penetration of D at 5 eV was distributed in depth up to 8 Å, and therefore the D atomic concentrations

$\frac{n_D}{n_C + n_B + n_O} x100\%$ were defined for the part of the computation cell from the top surface to 8 Å depth. The highest accumulated concentration of D reached was 43%, and this corresponds to

the D saturation at the considered impact energy (Fig. 3). Sufficient time (50 ps) was allowed for the evolution cascade, and the cell was thermalized and relaxed after each impact. After the computational cell was prepared, with some fraction of accumulated D, its replicas were then bombarded with 3100 independent 5 eV D trajectories, orthogonal to the surface, and at random locations at the surface. The results reported here were therefore obtained as the average from 3100 D trajectories. The retention chemistry of D evolves at the end of a collision cascade when the impact particle is thermalized which allowed comparison with the experimental results at higher impact energies [31]. We carried out the analysis of the resulting chemistry after the final rest location of each D impact, by performing the nearest-neighbor (NN) calculation for each atom in the surface, defining the coordination number of each atom and the nearest neighbors (NN) bond lengths [31,33]. The histograms of the NN bond lengths, and their cumulative distributions, normalized with the total number of retained D atoms out of 3100 impacts for a particular D accumulation (shown for example of a pristine surface in Fig. 4) were used in derivation of the average NN bond lengths

3. Results and Discussion

Previous studies on Li conditioning on ATJ graphite PFCs revealed the critical role that the relationship between oxygen, lithium, carbon and deuterium has in the reduced recycling and improved plasma performance associated with that conditioning technique [5,7,34].

In a similar manner, boron conditioning of PFCs leads to improve plasma performance. However, reduced physical and chemical sputtering yields, added to its oxygen gathering effect, are usually considered as the main reasons for its associated improvements [35–37]. CMD

simulations in addition to the *in-vacuuo* MAPP data, provided a new light on the mechanisms of oxygen and deuterium retention connected with boronization. The results presented in the sections 3.1 to 3.3 address these mechanisms and contribute to the conclusions previously established with the computational results and *in-vacuuo data.*

3.1 D_2^+ and Ar^+ irradiation XPS

Figure 5 shows the XPS data collected at three different stages of irradiation of the boronized ATJ sample. Figure 5(a) shows the B1s, C1s and O1s regions after irradiation with Ar^+ ions up to a fluence of $3.5x10^{17}$ ions.cm^{-2}. Although the data are not included in this work, the surface chemistry of the sample previous to the irradiation with Ar^+ is dominated by the presence of boron oxides clearly visible in the B1s and O1s region [24]. Similar chemical compositions were observed in samples exposed with the MAPP probe to boronizations and plasma exposures in NSTX-U [6,16].

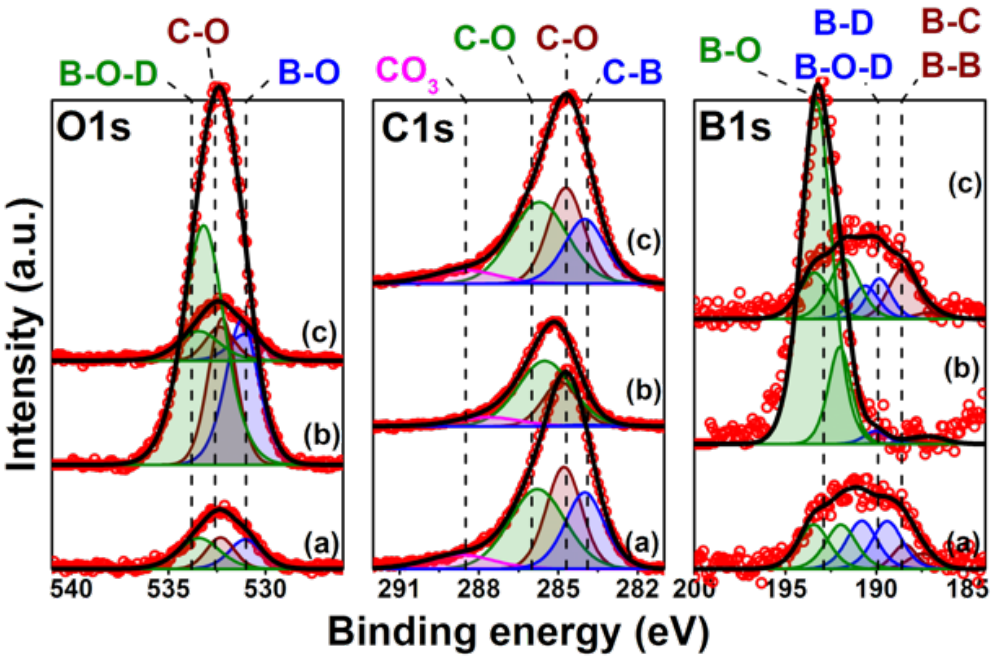

Figure 5. XPS spectra collected during the irradiation of the ATJ sample. Each region is labeled on the top, (a) is the spectra collected following the Ar^+ cleaning with $3.5x10^{17}$ ions.cm^{-2}, (b) shows the XPS data after a D_2^+ irradiation with $6.0x10^{16}$ ions.cm^{-2} and finally (c) shows the data after the sample was exposed to additional to an Ar^+ fluence of $2.0x10^{17}$ ions.cm^{-2}.

The Ar cleaning process relies on physical sputtering of the top monolayers of the material to initially remove contaminants attached to the surface during extraction, machining and transport of the cores, and secondly to remove layers of the material revealing the chemistry as a function of depth. In this way, the trace shown by figure 5a shows the surface chemistry after the removal of around 100 nm of material.

These traces have a close resemblance to those obtained shortly after a boronization in NSTX-U as it was revealed by *in-situ* measurements done with MAPP [6] i.e. low oxygen concentration and visible B-B and B-C interactions in the B1s region, including dominant B-D and B-O-D environments in the same region. Figure 5b shows the XPS data after two D_2^+ irradiations. It can be seen how now the surface is dominated by the presence of oxides; the areas

of the XPS envelopes in the B1s and O1s regions increase dramatically when compared with figure 5a. Additionally, the position of the envelope in the B1s region shifts towards higher binding energy as a consequence of the increase in the B-O peak area and the decrease in the B-C and B-B peaks. This behavior was observed in boronized surfaces with MAPP in addition to other laboratory controlled experiments [6,15,38,39].

This oxygen gettering effect of boron coatings has been used to explain the improved plasma performance observed after boronizations in different tokamaks. Interestingly, the oxygen surface concentration increase on the sample was only observed following deuterium irradiations. Exposures to argon beams did not induce any type of oxidation. The irradiations were conducted with the same plasma source and similar working pressures ($5x10^{-4}$ torr for Ar and 10^{-3} torr for D). Although in the context of plasma performance in tokamaks, the gettering effect of B might be more relevant, the mechanisms behind the increased oxygen concentration seen here are not isolated to only absorption of residual water vapor and oxygen catalyzed by the incoming ion flux. Phenomena as ion-induced segregation must be considered to justify the dramatic increased of O on the surface measured with XPS. Similar observations were made in the Li-C-O-D system as shown in figure 6 [5].

The oxidation of the B coatings, triggered by D_2^+ irradiations can be seen more clearly in figure 6. In this figure, the concentrations of O, B and C obtained after different irradiations are plotted as a function of the XPS measurement trial. For reference, the points 9, 12 and 14 correspond to the traces (a), (b) and (c) in figure 5 respectively. The point “0” shows the baseline

before argon cleaning. The oxygen removal effect of Ar^+ can be seen in the difference between points "0" and "1", there, the %O changes from 25 to 15%. The Ar^+ cleaning can be further observed as the irradiation continues from points "1" to "9", and the O% reduces from 15% to 5%, the total fluence used was $3.5x10^{17}$ cm^{-2} Ar^+. In contrast, the oxidation of the B coatings when irradiated with D_2^+ is shown by the trend that the concentrations follow between points "10" to "13". Three D_2^+ irradiations of equal fluence ($2x10^{16}$ cm^{-2}) were performed following "9".

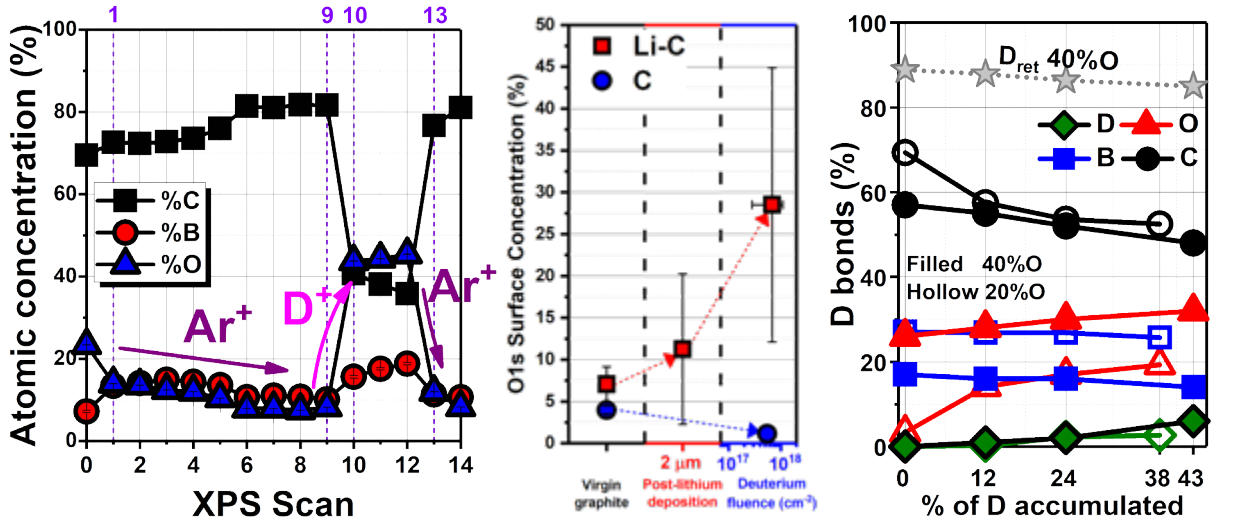

Figure 6. (a) Atomic concentrations of B, C and O in the sample obtained from XPS data. The data points are plotted as a function of the XPS trial and each point was obtained after an irradiation. "0" is the pre-irradiation baseline, points 1 through 9 were obtained in between Ar^+ irradiations, whereas points 10 to 12 were measured following D_2^+ exposures. Finally, points 13 and 14 were obtained after additional argon irradiations. (b) Shows similar data obtained with the Li-C-O-D system, plotted the O concentrations measured on carbon and lithiated carbon (pre and post irradiation with D_2^+) (reproduced from [5] with authorization from the publisher). (c) Percentage of deuterium bonds by component as obtained with the CMD-Reaxff simulations for various accumulated deuterium concentrations, for two cases of ratio of concentrations of O:B:C, 40:20:40 (filled symbols) and 20:20:60 (hollow symbols, [18]). Total retention is showed for the 40:20:40 case.

Following the first deuterium plasma exposure an abrupt change in the concentration of oxygen is seen, going from 5% to 42%. After this, the increments are considerably smaller with the irradiations i.e. ~3%. Finally, the concentration of oxygen was again reduced using an Ar^+

plasma. Points 13 and 14 were obtained with data collected following $1x10^{17}$ cm^{-2} irradiations at each point. These results clearly show how in boronized graphite, oxygen adsorption can be only driven under certain conditions, in this case, in the presence of energetic D_2^+ ions.

3.2 CMD Simulations

The CMD simulations performed on targets including B, C, O and D were performed using the approach described in section 2.3. The results for the D chemistry in the B-C-O-D surface are summarized in figure 6(c), where the percentage of total D bonds is plotted as a function of total deuterium concentration for each one of the involved species, and for two sets of atomic concentrations of the O, B and C species. The results were achieved by computing the nearest neighbors and their coordination numbers yielding the strongest favorable bond, as explained in Section 2.3, similarly as in [17]. As discussed in [18], the data for the atomic concentration ratio for O:B:C of 20:20:60 show favorable retention by the BCOD matrix compared with the rest of the configurations, followed by the BCO and CO cases, the lowest retention was obtained for the BC and C targets. For the case shown in Fig. 6c the D retentions decreases by more than 3% when D accumulation changes form 0% to the saturated one (43%) in O:B:C = 40:20:40. According to the simulations, the mechanism of D retention in oxidized-deuterated boronized carbon, varies with increasing D accumulation. As seen in figure 6c), initially, B binds most of the incident D when the surface contains same atomic concentrations of O and B (20%). Boron is more reactive than oxygen because of the so-called octet rule, i.e. a coordination number of four

is preferred for B atoms, and in our simulations we sometimes even find coordination numbers of five and six, enabling larger number of D to bond to a B atom than to oxygen (with typical coordination number 2). Also, electron withdrawing ligands on B such as O further increase D uptake on B. The role of B in the retention of D does not change with increasing D accumulation, although it is suppressed with increase of O atomic concentration. However, as the concentration of D increases, this D bonded to B slightly decreases and the additional deuterium attaches to the oxygen atoms in the target, reducing both the role of carbon and boron in the retention. In this way, the role of oxygen becomes more important when the number of D atoms raises in the sample, and at 38% D concentration for O:B;C=20:20:60 O binds almost the same amount as B, i.e. ~20% [17,40]. Interestingly, the similar trends are also seen when O atomic concentration is set 40% (and B 20%). The difference is that the oxygen in this case plays more important role in bonding D even for 0% of accumulated D, while at 43% of D oxygen is as twice effective in bonding D than boron. The increases and decreases of the roles of oxygen and boron, respectively, with accumulation of D show the same rate of change for both 40% and 20 % of O cases

3.3 Correlating ion-induced desorption to surface chemistry in-operando

The emission of different species from the sample, and their presence in the analysis chamber, in addition to other gas species, were monitored with a QMS. Complementarily, the ion flux, incident to the sample during the different irradiations was measured *in-situ,* with a nano-amp

meter controlled via serial port. Figure 7 shows the data collected with the RGA and the amp-meter during four different irradiations.

Figure 7 shows the partial pressure of different gases as a function of the irradiation time, the plot also displays the ion flux incident on the sample (red transparent line in 7(a) and 7(b) and purple transparent line in 7(c) and 7(d)). The time coincidence of specific partial masses measured by the mass spectrometer during irradiation combined with *in-situ in-operando* surface chemistry characterization enables direct correlations of ion-induced dynamic mechanisms that drive chemical phase transformations. Although ultimately these mass spectrometry measurements can provide estimates of chemical sputtering, quantitative analysis is necessary and beyond the scope of this paper. Figures 7(a) and 7(b) show the data collected during two deuterium irradiations. The spectra are dominated by neutral species used to feed the plasma in this case deuterium (the partial pressure of D_2 is around 10^{-8} Torr, not shown in the figures), additionally the partial pressure of water (18 amu) is relatively high compared with other masses. However, no masses are strongly responsive to the ion flux, but their partial pressure is a stronger function of the gas feed pressure.

In figure 7(b), nitrogen (N and N_2), oxygen (O and O_2) and the CD_4 masses show a small increase in partial pressure starting around 13 min into the irradiation, the reason for this smooth rise is still under investigation, however, temperature driven desorption (due to heating through irradiation) has been discarded, since temperature measurements obtained under similar irradiation conditions yielded increments between 2-3^{o}C from room temperature.

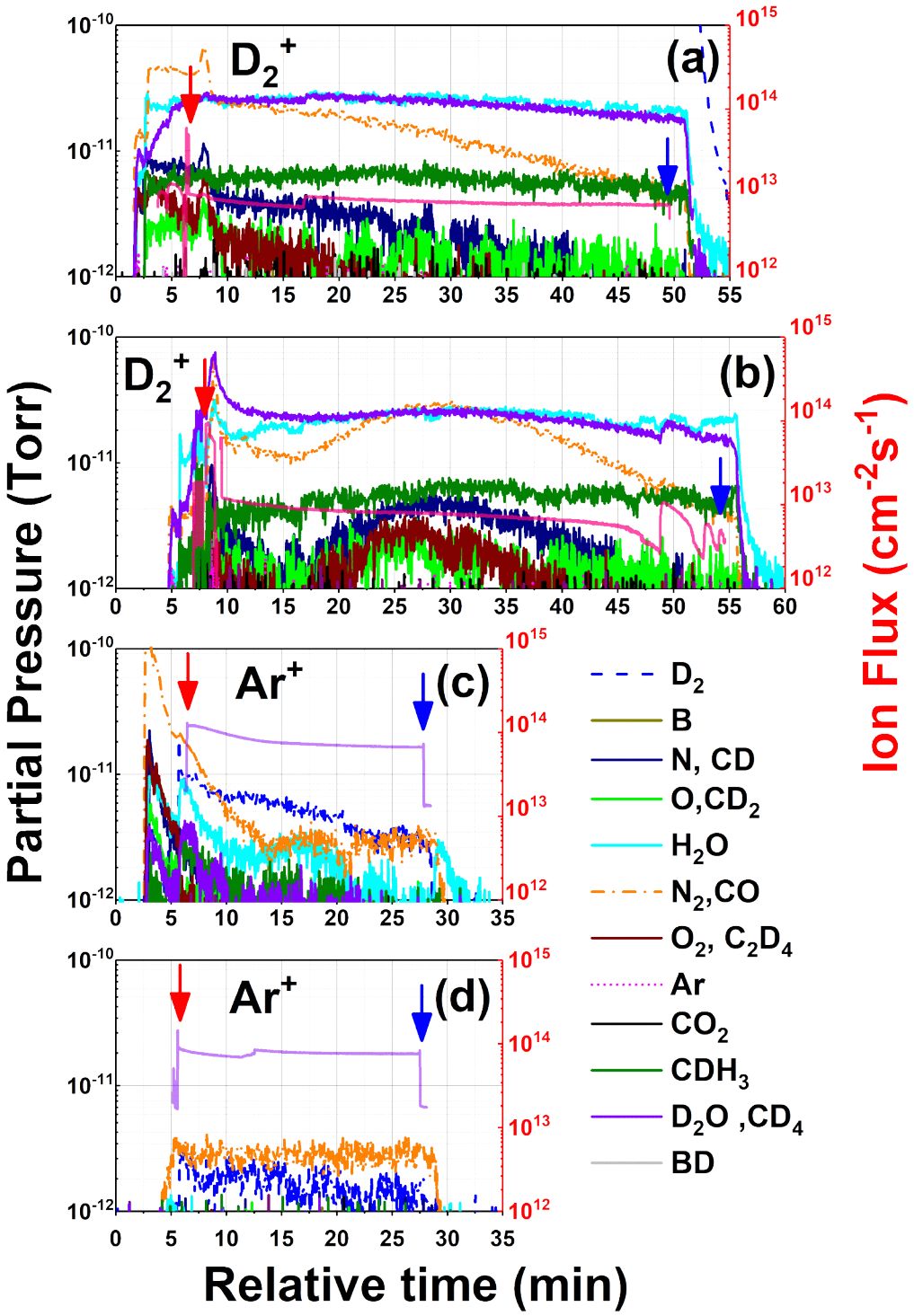

Figure 7. Residual gas analysis spectra collected during two deuterium and two Ar sequential irradiations plotted as a function of time. The right axes refer to the partial pressure of each gas species as indicated by the label on the left. The left axis indicates the magnitude of the ion flux in cm^{-2}. s^{-1}, this quantity is plotted with a red line in panels (a) and (b) and a purple line in panels (c) and (d). Panels (a) and (b) show D_2^+ irradiations of $2x10^{16}$ cm^{-2} total fluence, and panels (c) and (d) show Ar^+ irradiations with total fluences of $1x10^{17}$ cm^{-2}.In all the cases, the beginning of the irradiation is signaled with a red arrow, whereas the end is marked with a blue arrow.

Figures 7(c) and 7(d) show the partial pressure of gasses during two Ar^+ irradiations. In these two cases, the spectra are also dominated by the neutral species inserted in the analysis chamber through the gas feed line i.e. Ar (argon partial pressure is ~10^{-9} Torr during the irradiations). Remarkably, the figures show how the D_2 mass is responsive to the ion flux measured on the sample, since, in both figures, this trace spikes up following the ion flux signal, again, in both cases around 5 minutes after the start of the irradiation. In the same way, in these figures, the value of the partial pressure of D_2 decreases steadily during both irradiations, starting close to $1x10^{-11}$ Torr in figure 4(c) and registering ~$1x10^{-12}$ Torr at the end of the irradiation shown in figure 6(b).

We hypothesize that the decreasing D_2 and D_2O partial pressure in figures 7(c) and 7(d) are evidence of deuterium retention by the oxide-boron layers on the graphite sample. As shown in figures 5 and 6 and as discussed in section 3.1, deuterium irradiation on boronized graphite, drives the oxidation of the surface, simultaneously, these freshly formed oxides retain upcoming deuterium molecules and atoms. The data shown in section 3.1 also shows how irradiation with Ar^+ removes the surface oxides, thus removing the retained deuterium as shown by the data in figure 7.

Conclusions

We irradiated samples manufactured from tiles extracted from NSTX-U with D and Ar ions using low fluences at 250 eV/amu and 1000 eV respectively. To analyze the effect of these irradiations on the chemistry of the samples, we used *in-situ* XPS analysis in between the plasma exposures, additionally, we performed mass spectrometry analysis of the ion-induced desorption correlated to the irradiations and surface characterization *in-operando* and *in-situ* to monitor the emission of impurities. In-situ XPS data shows that irradiation with argon removes contamination and oxides from the surface of the sample, in this case, a total fluence of $3.5x10^{17}cm^{-2}$ reduced the oxygen concentration in the sample around 15%. In contrast, the irradiation with deuterium ions, using a fluence approximately one order of magnitude less than that of Ar i.e. $6.0x10^{16}cm^{-2}$, increased the oxygen concentration in the sample to 45%. We made similar observations in NSXT-U with the MAPP probe [6,24], were progressive oxidation of boronized graphite was observed *in-vacuo.* Argon ions were later used on the sample again, removing the previously increased oxygen concentration. According to the mass spectrometry spectra collected, we deduce the oxidized boron coatings are able to retain deuterium under the conditions of our experiment. We conclude this since, the partial pressure of the m/q ratio corresponding to D_2 and D_2O show a strong dependence on Ar^+ flux measured at the sample following two deuterium irradiations. Hence, the mechanisms can be summarized as follows; initial irradiation with D_2^+ induces the oxidation of the boronized graphite (catalyzing residual water vapor adsorption and ion-induced segregation of retained oxygen towards the surface of the sample), similar to the case of Li coatings on carbon [5,18,41] and promotes the implantation of weakly bonded D atoms on

the surface, as a consequence the O% drastically increases. These oxides are latter removed with Ar^+, the sputtered oxide layers leave the surface of the sample carrying the attached D atoms thus increasing their partial pressure in the vacuum. Since the amount of implanted or deposited deuterium atoms is dictated by the relatively low fluence used, the partial pressure of this gas decreases almost linearly with time during the Ar irradiations, and is smaller in the second exposure than in the first one.

These measurements and analysis elucidate understanding of the mechanisms behind the improvements on plasma performance that B conditioning has, and, are congruent with the observations made *in-vacuo* with the MAPP probe. In this sense, the set of measurements presented here provides a confirmation under a more controlled isolated experimental basis of the measurements obtained on site with the MAPP.

CMD simulations show that deuterium retention chemistry in the BCOD system depends on the total amount of D implanted in the sample, as well as on the concentration of oxygen. According to the data, when atomic concentration of oxygen is the same to that of boron (i.e. 20%), oxygen only has a relevant role in trapping deuterium at high concentrations of D in the sample. However, if concentration of oxygen is set to 40%, double to the concentration of boron in the sample, oxygen is suppressing the role of B in the D-bonding chemistry even for 0% of D, and this suppression increases with D accumulation. In the case of NSTX-U, an increased concentration of D comes with increments in the concentration of O, as shown in section 3.1 and in Ref [6,24]. This raise in the concentration of oxygen affects the sputtering properties of the

PFC, since the yield varies from 0.122 for a target with 7.0% O to 0.161 for one with 40% O concentration when irradiated with 1.0 keV Ar^+ ions. Furthermore the yields for preferential sputtering predict 0.024 for B, 0.045 for C and 0.096 for O under the same irradiation conditions[10], as a consequence, the emission of oxygen (and any D bond to it) from the surface would decrease the plasma performance by increasing radiation loses (and increasing recycling). Such observations were also made in NSTX-U with the MAPP probe [6].

Acknowledgments

This work was supported by the DOE-OFES collaborative grant DE-SC0014264 (FB), DOE OFES grant DOE DE-SC0010717 (JPA), by the A. von Humboldt Foundation for research fellowship (FJDG) and by the USDOE FES Grant No. DE-SC0013752 (PSK). The CMD calculations reported in this paper were performed at the IACS/SBU institutional cluster Seawulf.

References

[1] F. Dobran, Fusion energy conversion in magnetically confined plasma reactors, Prog. Nucl. Energy. 60 (2012) 89–116. doi:10.1016/j.pnucene.2012.05.008.

[2] J. Wesson, Tokamaks, 4th ed., Oxford University Press, New York, NY, 2011.

[3] J. Winter, Wall conditioning in fusion devices and its influence on plasma performance, Plasma Phys. Control. Fusion. 38 (1996) 1503. doi:10.1088/0741-3335/38/9/001.

[4] G. Federici, C.H. Skinner, J.N. Brooks, J.P. Coad, C. Grisolia, A.A. Haasz, A. Hassanein, V. Philipps, C.S. Pitcher, J. Roth, W.R. Wampler, D.G. Whyte, Plasma-material interactions in current tokamaks and their implications for next step fusion reactors, Nucl. Fusion. 41 (2001) 1967–2137. doi:10.1088/0029-5515/41/12/218.

[5] C.N. Taylor, J. Dadras, K.E. Luitjohan, J.P. Allain, P.S. Krstic, C.H. Skinner, The role of oxygen in the uptake of deuterium in lithiated graphite, J. Appl. Phys. 114 (2013) 223301. doi:10.1063/1.4841115.

[6] F. Bedoya, J.P. Allain, R. Kaita, C.H. Skinner, B.E. Koel, F. Scotti, Initial studies of plasma facing component surface conditioning in the national spherical tokamak experiment upgrade with the materials analysis particle probe, Nucl. Mater. Energy. 12 (2017) 1248–1252. doi:10.1016/j.nme.2017.03.035.

[7] R. Maingi, S.M. Kaye, C.H. Skinner, D.P. Boyle, J.M. Canik, M.G. Bell, R.E. Bell, T.K. Gray, M.A. Jaworski, R. Kaita, H.W. Kugel, B.P. LeBlanc, D.K. Mansfield, T.H. Osborne, S.A. Sabbagh, V.A. Soukhanovskii, Continuous Improvement of H-Mode Discharge Performance with Progressively Increasing Lithium Coatings in the National Spherical Torus Experiment, Phys. Rev. Lett. 107 (2011). doi:10.1103/PhysRevLett.107.145004.

[8] C. Hollenstein, B.P. Duval, T.D. de Wit, B. Joye, H.J. Künzli, P. Oelhafen, R. Zehringer, R. Hauert, E.M. Moser, Cold boronisation in TCA, J. Nucl. Mater. 176 (1990) 343–349. doi:10.1016/0022-3115(90)90070-4.

[9] J. Winter, Tokamak wall coatings, Plasma Phys. Control. Fusion. 36 (1994) B263. doi:10.1088/0741-3335/36/12B/022.

[10] F.J. Domínguez-Gutiérrez, P.S. Krstić, Chemical sputtering of boronized and oxidized carbon surfaces irradiated by low-energy deuterium atoms, J. Appl. Phys. 121 (2017) 215302. doi:10.1063/1.4984756.

[11] F.J. Domínguez-Gutiérrez, P.S. Krstić, Sputtering of lithiated and oxidated carbon surfaces by low-energy deuterium irradiation, J. Nucl. Mater. 492 (2017) 56–61. doi:10.1016/j.jnucmat.2017.05.014.

[12] D.J. Battaglia, M.D. Boyer, S.P. Gerhardt, D. Mueller, C.E. Myers, W. Guttenfelder, J.E. Menard, S.A. Sabbagh, F. Scotti, F. Bedoya, R.E. Bell, J. Berkery, A. Diallo, N. Ferraro, S.M. Kaye, M.A. Jaworski, B.P. LeBlanc, M. Ono, J.-K. Park, M. Podesta, R. Raman, V. Soukhanovskii, Scenario development during commissioning operations on the National Spherical Torus Experiment Upgrade, Nucl. Fusion. (2018). doi:10.1088/1741-4326/aaa6e0.

[13] J.E. Menard, J.P. Allain, D.J. Battaglia, F. Bedoya, R.E. Bell, E. Belova, J.W. Berkery, M.D. Boyer, N. Crocker, A. Diallo, F. Ebrahimi, N. Ferraro, E. Fredrickson, H. Frerichs, S. Gerhardt, N. Gorelenkov, W. Guttenfelder, W. Heidbrink, R. Kaita, S.M. Kaye, D.M. Kriete, S. Kubota, B.P. LeBlanc, D. Liu, R. Lunsford, D. Mueller, C.E. Myers, M. Ono, J.-K. Park, M. Podesta, R. Raman, M. Reinke, Y. Ren, S.A. Sabbagh, O. Schmitz, F. Scotti, Y. Sechrest, C.H. Skinner, D.R. Smith, V. Soukhanovskii, T. Stoltzfus-Dueck, H. Yuh, Z. Wang, I. Waters, J.-W. Ahn, R. Andre, R. Barchfeld, P. Beiersdorfer, N. Bertelli, A. Bhattacharjee, D. Brennan, R. Buttery, A. Capece, G. Canal, J. Canik, C.S. Chang, D. Darrow, L. Delgado-Aparicio, C. Domier, S. Ethier, T. Evans, J. Ferron, M. Finkenthal, R. Fonck, K. Gan, D. Gates, I. Goumiri, T. Gray, J. Hosea, D. Humphreys, T. Jarboe, S. Jardin, M.A. Jaworski, B. Koel, E. Kolemen, S. Ku, R.J. La Haye, F. Levinton, N. Luhmann, R. Maingi, R. Maqueda, G. McKee, E. Meier, J. Myra, R. Perkins, F. Poli, T. Rhodes, J. Riquezes, C. Rowley, D. Russell, E. Schuster, B. Stratton, D. Stutman, G. Taylor, K. Tritz, W. Wang, B. Wirth, S.J. Zweben, Overview of NSTX Upgrade initial results and modelling highlights, Nucl. Fusion. 57 (2017) 102006. doi:10.1088/1741-4326/aa600a.

[14] M. Ono, J. Chrzanowski, L. Dudek, S. Gerhardt, P. Heitzenroeder, R. Kaita, J.E. Menard, E. Perry, T. Stevenson, R. Strykowsky, P. Titus, A. von Halle, M. Williams, N.D. Atnafu, W. Blanchard, M. Cropper, A. Diallo, D.A. Gates, R. Ellis, K. Erickson, J. Hosea, R. Hatcher, S.Z. Jurczynski, S. Kaye, G. Labik, J. Lawson, B. LeBlanc, R. Maingi, C. Neumeyer, R. Raman, S. Raftopoulos, R. Ramakrishnan, A.L. Roquemore, S.A. Sabbagh, P. Sichta, H. Schneider, M. Smith, B. Stratton, V. Soukhanovskii, G. Taylor, K. Tresemer, A. Zolfaghari, The NSTX-U Team, Progress toward commissioning and plasma operation in NSTX-U, Nucl. Fusion. 55 (2015) 073007. doi:10.1088/0029-5515/55/7/073007.

[15] C.H. Skinner, F. Bedoya, F. Scotti, J.P. Allain, W. Blanchard, D. Cai, M. Jaworski, B.E. Koel, Advances in boronization on NSTX-Upgrade, Nucl. Mater. Energy. 12 (2017) 744–748. doi:10.1016/j.nme.2016.11.024.

[16] F. Bedoya, J.P. Allain, R. Kaita, C.H. Skinner, L. Buzi, B.E. Koel, Unraveling wall conditioning effects on plasma facing components in NSTX-U with the Materials Analysis Particle Probe (MAPP), Rev. Sci. Instrum. 87 (2016) 11D403. doi:10.1063/1.4955276.

[17] F.J. Domínguez-Gutiérrez, F. Bedoya, P.S. Krstić, J.P. Allain, S. Irle, C.H. Skinner, R. Kaita, B. Koel, Unraveling the plasma-material interface with real time diagnosis of dynamic boron conditioning in extreme tokamak plasmas, Nucl. Fusion. 57 (2017) 086050. doi:10.1088/1741-4326/aa7b17.

[18] C.N. Taylor, J.P. Allain, K.E. Luitjohan, P.S. Krstic, J. Dadras, C.H. Skinner, Differentiating the role of lithium and oxygen in retaining deuterium on lithiated graphite plasma-facing componentsa), Phys. Plasmas 1994-Present. 21 (2014) 057101. doi:10.1063/1.4874340.

[19] C.N. Taylor, K.E. Luitjohan, B. Heim, L. Kollar, J.P. Allain, C.H. Skinner, H.W. Kugel, R. Kaita, A.L. Roquemore, R. Maingi, Surface chemistry analysis of lithium conditioned NSTX graphite tiles correlated to plasma performance, Fusion Eng. Des. 88 (2013) 3157–3164. doi:10.1016/j.fusengdes.2013.09.007.

[20] R.A. Pitts, J.P. Coad, D.P. Coster, G. Federici, W. Fundamenski, J. Horacek, K. Krieger, A. Kukushkin, J. Likonen, G.F. Matthews, M. Rubel, J.D. Strachan, J.-E. contributors, Material erosion and migration in tokamaks, Plasma Phys. Control. Fusion. 47 (2005) B303–B322. doi:10.1088/0741-3335/47/12B/S22.

[21] G.F. Matthews, Material migration in divertor tokamaks, J. Nucl. Mater. 337–339 (2005) 1–9. doi:10.1016/j.jnucmat.2004.10.075.

[22] SPECS, Components for Surface Analysis PHOIBOS 150 NAP, SPECS, Germany, 2010. http://www.specs.de/cms/upload/PDFs/SPECS_Prospekte/2010_11_PHOIBOS_150_NAP_product_brochure_final_web.pdf (accessed March 19, 2017).

[23] Tectra, Plasma source operating manual Gen II Plasma source, Tectra, Frankfurt, 2012.

[24] F. Bedoya, PLASMA FACING COMPONENTS CONDITIONING TECHNIQUES AND THEIR CORRELATION WITH PLASMA PERFORMANCE IN THE NATIONAL SPHERICAL TORUS EXPERIMENT UPGRADE (NSTX-U), PhD, University of Illinois at Urbana-Champaign, 2017.

[25] M. Nieto-Perez, J.P. Allain, B. Heim, C.N. Taylor, Chemical and physical erosion of carbon and metallic substrates containing lithium during low-energy deuterium ion irradiation, J. Nucl. Mater. 415 (2011) S133–S136. doi:10.1016/j.jnucmat.2010.10.078.

[26] A.C.T. van Duin, S. Dasgupta, F. Lorant, W.A. Goddard, ReaxFF: A Reactive Force Field for Hydrocarbons, J. Phys. Chem. A. 105 (2001) 9396–9409. doi:10.1021/jp004368u.

[27] M.R. Weismiller, A.C.T. van Duin, J. Lee, R.A. Yetter, ReaxFF Reactive Force Field Development and Applications for Molecular Dynamics Simulations of Ammonia Borane Dehydrogenation and Combustion, J. Phys. Chem. A. 114 (2010) 5485–5492. doi:10.1021/jp100136c.

[28] S. Plimpton, Fast Parallel Algorithms for Short-Range Molecular Dynamics, J. Comput. Phys. 117 (1995) 1–19. doi:10.1006/jcph.1995.1039.

[29] W.J. Mortier, S.K. Ghosh, S. Shankar, Electronegativity-equalization method for the calculation of atomic charges in molecules, J. Am. Chem. Soc. 108 (1986) 4315–4320. doi:10.1021/ja00275a013.

[30] Y. Cong, Z.-Z. Yang, General atom-bond electronegativity equalization method and its application in prediction of charge distributions in polypeptide, Chem. Phys. Lett. 316 (2000) 324–329. doi:10.1016/S0009-2614(99)01289-0.

[31] P. Krstic, J. Allain, C. Taylor, J. Dadras, S. Maeda, K. Morokuma, J. Jakowski, A. Allouche, C. Skinner, Deuterium Uptake in Magnetic-Fusion Devices with Lithium-Conditioned Carbon Walls, Phys. Rev. Lett. 110 (2013). doi:10.1103/PhysRevLett.110.105001.

[32] Zheng Guishan, Lundberg Marcus, Jakowski Jacek, Vreven Thom, Frisch Michael J., Morokuma Keiji, Implementation and benchmark tests of the DFTB method and its application in the ONIOM method, Int. J. Quantum Chem. 109 (2009) 1841–1854. doi:10.1002/qua.22002.

[33] P.S. Krstic, J.P. Allain, A. Allouche, J. Jakowski, J. Dadras, C.N. Taylor, Z. Yang, K. Morokuma, S. Maeda, Dynamics of deuterium retention and sputtering of Li–C–O surfaces, Fusion Eng. Des. 87 (2012) 1732–1736. doi:10.1016/j.fusengdes.2011.07.009.

[34] F.J. Dominguez, F. Bedoya, P.S. Krstic, J.P. Allain, S. Irle, C.H. Skinner, R. Kaita, B.E. Koel, Deuterium uptake in boronized ATJ graphite walls of NSTX, Phys. Rev. Lett. (2016).

[35] O. Buzhinskij, Y. Semenets, Review of in situ boronization in contemporary tokamaks, Fusion Technol. 32 (1997) 1–13.

[36] C.H. Skinner, H.W. Kugel, R. Maingi, W.R. Wampler, W. Blanchard, M.G. Bell, R.E. Bell, D.A. Gates, S.M. Kaye, P. LaMarche, Effect of boronization on ohmic plasmas in NSTX, Nucl. Fusion. 42 (2002) 329. http://iopscience.iop.org/0029-5515/42/3/313 (accessed March 7, 2013).

[37] J. Winter, H.G. Esser, L. Könen, V. Philipps, H. Reimer, J. v. Seggern, J. Schlüter, E. Vietzke, F. Waelbroeck, P. Wienhold, T. Banno, D. Ringer, S. Vepřek, Boronization in textor, J. Nucl. Mater. 162–164 (1989) 713–723. doi:10.1016/0022-3115(89)90352-8.

[38] V.K. Alimov, R.K. Zalavutdinov, B.M.U. Scherzer, Oxygen retention in D-ion-irradiated B 4 C and boron-doped graphites, J. Nucl. Mater. 212 (1994) 1461–1466. http://www.sciencedirect.com/science/article/pii/0022311594910707 (accessed March 26, 2016).

[39] R. Zehringer, H. Künzli, P. Oelhafen, C. Hollenstein, Oxidation behaviour of boron carbide, J. Nucl. Mater. 176 (1990) 370–374. doi:10.1016/0022-3115(90)90074-W.

[40] F.J. Domínguez-Gutiérrez, F. Bedoya, P.S. Krstic, J.P. Allain, A.L. Neff, K. Luitjohan, Studies of lithiumization and boronization of ATJ graphite PFCs in NSTX-U, Nucl. Mater. Energy. (n.d.). doi:10.1016/j.nme.2016.12.028.

[41] C.N. Taylor, B. Heim, J.P. Allain, Chemical response of lithiated graphite with deuterium irradiation, J. Appl. Phys. 109 (2011) 053306. doi:10.1063/1.3555097.